FINAL REPORT FOR

DOE/NSF Grant No. DE-SC0008333

"Collaborative Research: Atmospheric Pressure Microplasma Chemistry-Photon Synergies"

Submitted by

J. G. Eden
S.-J. Park

Department of Electrical and Computer Engineering
University of Illinois
306 North Wright St.
Urbana, IL 61801

December 2015

I. Overview and Summary of Accomplishments

Combining the effects of low temperature, atmospheric pressure microplasmas and microplasma photon sources offers the promise of greatly expanding the range of applications for each of them. The plasma sources create active chemical species and these can be activated further by the addition of photons and the associated photochemistry. There are many ways to combine the effects of plasma chemistry and photochemistry, especially if there are multiple phases present. This project combined the construction of appropriate test experimental systems, various spectroscopic diagnostics and mathematical modeling.

Through a continuous discussion and co-design process with the UC-Berkeley Team, we have successfully completed the fabrication and testing of all components for a microplasma array-assisted system designed for photon-activated plasma chemistry research. Microcavity plasma lamps capable of generating more than 20 mW/cm^2 at 172 nm (Xe dimer) were fabricated with a custom form factor to mate to the plasma chemistry setup, and a lamp was current being installed by the Berkeley team so as to investigate plasma chemistry-photon synergies at a higher photon energy (~7.2 eV) as compared to the UVA treatment that is afforded by UV LEDs operating at 365 nm. In particular, motivated by the promising results from the Berkeley team with UVA treatment, we also produced the first generation of lamps that can generate photons in the 300-370 nm wavelength range. Another set of experiments, conducted under the auspices of this grant, involved the use of plasma microjet arrays. The combination of the photons and excited radicals produced by the plasma column resulted in broad area deactivation of bacteria.

II. Plasma Chemistry and Photon Synergies at the University of Illinois at Urbana-Champaign (UIUC)

A. Plasma Chemistry

Microplasma jet arrays developed at UIUC provide simultaneously both optical radiation and plasma-produced radicals, as exemplified by the results of Fig. 1. The photograph at left shows a 5 × 5 array of plasma jets produced in helium feedstock gas by cylindrical electrodes embedded within a block of moldable polymer. These 25 plasma jets interact with ambient air to produce an obvious violet glow that is emitted by the nitrogen molecular ion. A representative spectrum of the emission produced by the array is shown at right in Fig. 1- emission from the molecular ion at 391.4 nm clearly dominates the spectrum. These data demonstrate that specific ions (or radicals) can be produced by microplasma sources, thereby enabling a surface to be dosed selectively with a particular species and/or controlled photon energies.

A brief description of the design and performance of the microplasma jet arrays employed in these experiments is given here, as are the experimental results, obtained in collaboration with the group of Prof. Michael Kong at Old Dominion University. End-on and plan views of the structure of a 4 × 4 array of microplasma jets are presented in panels (a) and (b), respectively, of figure 2. Fabricated in a flexible silicone polymer, this array structure has an overall volume of 10 × 10 × 4 mm^3. For all of the experiments reported here, the microchannel diameter (D_c) and pitch (center-to-center spacing) along the vertical coordinate (L_{co}) were fixed

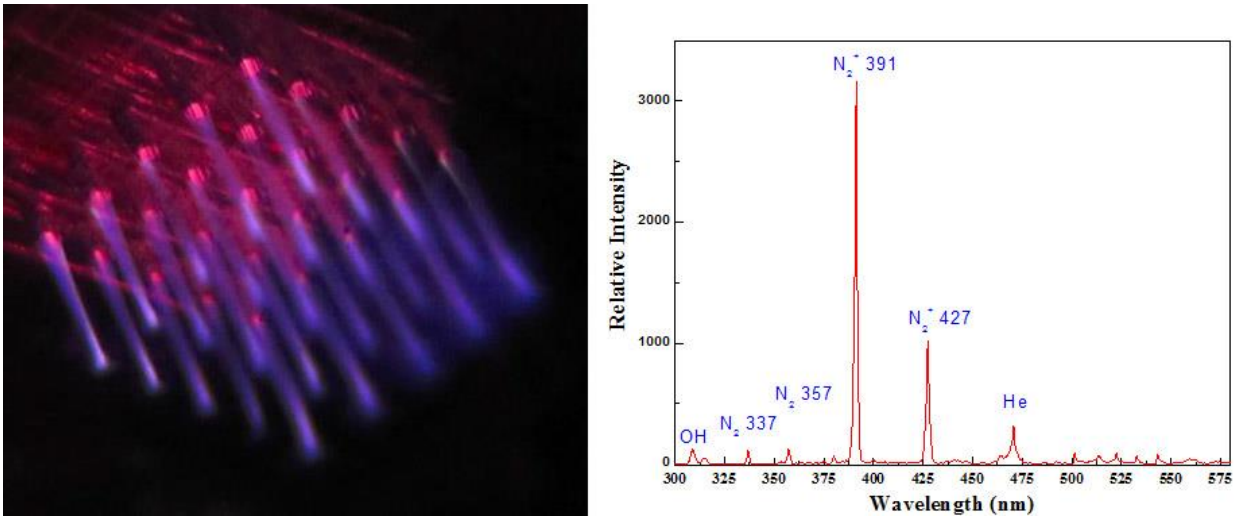

Fig. 1 (Left) Photograph of a 5x5 array of microchannel plasma jets, produced in He feedstock gas and expanding into ambient air; (Right) Representative spectrum (in the visible and UV) of the emission shown at left. The dominant features originate from the nitrogen dimer ion.

at 355 µm and 1 mm, respectively. However, the channel pitch along the horizontal coordinate (L_{cp}) was varied between 0.5 mm and 2 mm, which corresponds to jet packing densities in these arrays of 60 – 240 cm^{-2} in the plane defined by the microchannel exit apertures. Since the diameter of the electrode wire is 255 µm, the distance from an electrode to the wall of the nearest microchannel is 195 µm. In view of the microchannel separations (pitch) mentioned above, one concludes that the radial expansion of the bactericidal effect arising from a single jet is unlikely to perturb that produced by an adjacent plasma column if jet-jet interactions are negligible. Research grade helium served as the feedstock gas and the flow rate was maintained at 0.625 standard liters per minute (slm) throughout the experiments. Powered by a 23 kHz sinusoidal voltage having an RMS magnitude of 1 kV, the array was operated with all plasma jets ignited (although the capability for individually addressing the jets is available), and the array was positioned such that the microchannel exit plane was 4 mm from an agar plate lying within a 6 cm diameter Petri dish. Panel (c) of Fig. 2 is a photograph of the 4 × 4 array in operation and impinging on the agar plate which was electrically grounded. The jets are observed to be uniform in cross-section from jet-to-jet, and a flattening of each plasma plume as it arrives at the agar plate is evident. While electrostatic interactions among different plasma jets is inevitable, the images obtained of the arrays tested throughout this work (such as that of Fig. 1(c)) suggest that their influence on the collimation characteristics of these dense microplasma jet arrays appears to be minimal.

Classical plasma diagnostics are capable of measuring absolute concentrations of a variety of the radicals and atomic species present in non-equilibrium, atmospheric pressure plasmas. For instance, the number densities of ground and excited state nitric oxide (NO), hydroxyl (OH) and atomic oxygen (O) are often determined or estimated with laser-based diagnostics. However, it is neither practical nor possible at present to measure the absolute concentrations of all the species in a plasma that drive a biological or materials process of interest. In fact, at least a few of the species responsible for a specific plasma-initiated treatment are frequently not known or identified. For many applications of atmospheric plasmas, it appears that the efficacy of the process is often facilitated synergistically by multiple plasma species. In short, the identities of the plasma species

underlying the plasma processes of greatest interest, and the threshold number densities required to drive a specific process, are often unknown. As a result, a focus on one or a few reactive plasma species that may be accessible optically, but without clear application context, is of limited scientific and practical value.

An unconventional and novel diagnostic is, therefore, desirable to monitor the gas phase chemistry triggered by low temperature plasmas, and to do so in the context of a specific application. For biomedical effects of atmospheric pressure plasmas, one such diagnostic was reported in which bacterial mutants responsible for DNA and lipid oxidation damage are deactivated. A comparison of the rate of plasma-induced inactivation of these bacterial mutants, in comparison with that for their wild type, can be used to identify the relative importance of different plasma species. We conclude that bacterial inactivation can serve as a novel and broad diagnostic of the reactive oxygen species (ROS), and other long-lived radicals and ions, generated by low temperature plasmas within or external to the plasma itself. It is obvious that bacterial inactivation also provides a sensitive detector of those plasma conditions under which the gas phase number densities of critical reactive species have exceeded the threshold for bacterial inactivation, even if the numerical value for the threshold concentration may remain unknown. Insofar as the investigation of potential chemical coupling between individual plasma jets in an array is concerned, this approach provides spatial resolution in two dimensions when a lawn of bacterial cells acts as the substrate for an array of plasma jets. Each sample treated by the arrays in the present experiments is a lawn of the bacterium *E. coli* K12 prepared on a 6 cm diameter Petri dish with an initial cell concentration of ~1.2x10^5 cm^{-2}. Such a large cell density is useful in order to observe both the antibacterial effects of individual plasma jets, as well as jet-jet interactions. Bacterial inactivation is quantified by transfecting the *E. coli* K12 cells with green fluorescence protein (GFP) *Sox*-promoter plasmid.

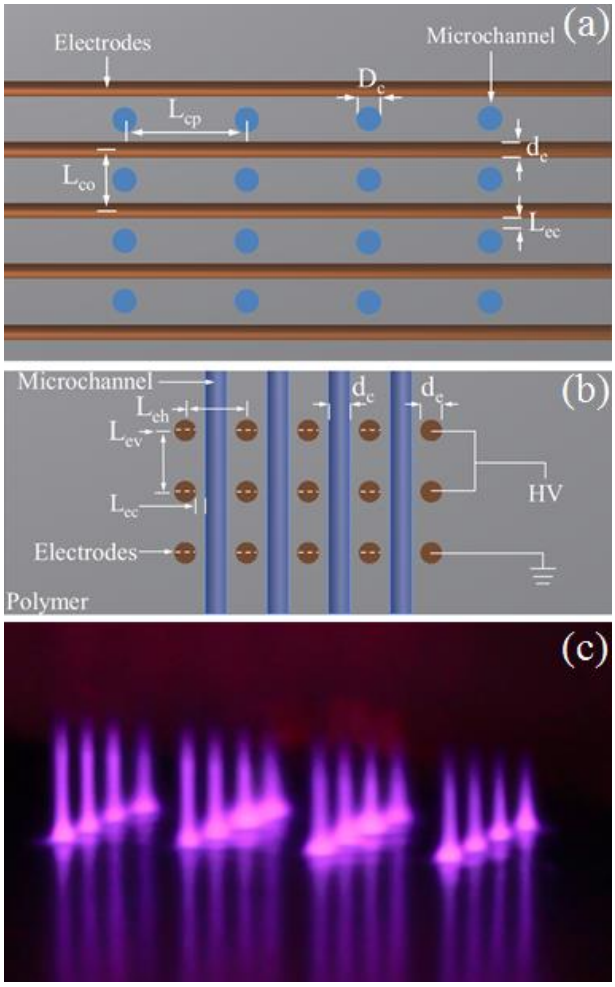

Figure 2: Design and operation of a 4×4 array of low temperature microplasma jets: (a) end-on view of the array, illustrating several dimensions of the structure and one set of electrodes oriented parallel to the plane defined by the microchannel apertures; (b) top view of the array, as well as a few of the electrical connections; (c) photograph of a 4 × 4 microplasma array exiting from the assembly (at top) and impinging on an electrically-grounded, agar plate. The reflection of the jets in the plate is evident, and the He gas flow through each microchannel was set at 0.625 slm. The applied voltage to the electrodes had an RMS value of 1kV at 23 kHz.

Sox is a gene that prevents oxidation by hydrogen peroxide, and its expression via its promoter plasmid is indicated by GFP fluorescence. Cell transfection with GFP promoter follows the standard protocol and the fluorescence produced when transfected cells are photoexcited at 483 nm (with a filtered lamp) serves as a measure of the active *E. coli* population. Extinction of the green fluorescence, however, is an indicator of bacterial inactivation by any chemical or physical process. Because GFP-transfected bacteria are weaker than their non-transfected counterparts, experiments were also conducted in which normal *E. coli* K12 cells were treated with the microplasma arrays. Microscopic images of the treated samples show a clear contrast in gray scale between those areas where the bacteria are inactivated and those in which they are not.

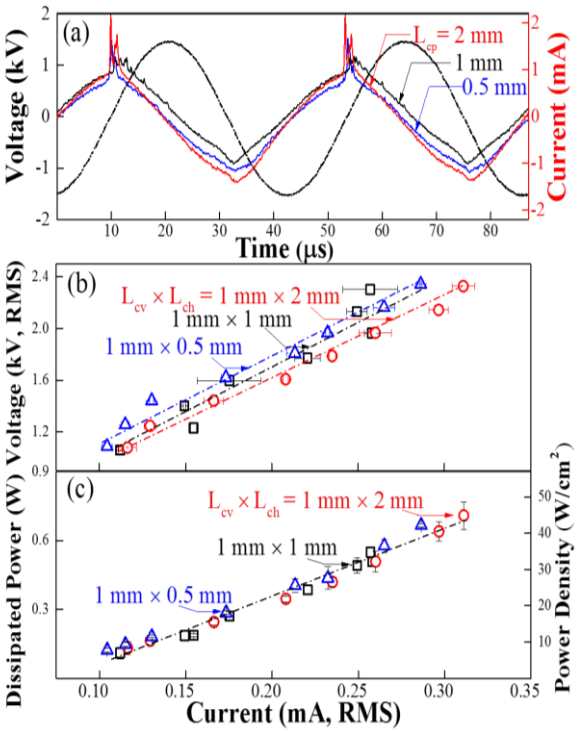

Figure 3. Electrical characteristics of the plasma jet array of Fig 1 when the microchannel pitch along the horizontal axis of Figure 1a (L_{cp}) is 0.5, 1.0 and 2.0 mm: (a) voltage and current waveforms; (b) voltage-current characteristic, and (c) current dependence of the power dissipated in the 16 jet array.

Several electrical characteristics of the arrays are illustrated in figure 3 for horizontal microchannel pitch values of L_{cp} = 0.5, 1.0, and 2.0 mm. Current and voltage waveforms, shown in Fig. 2a, exhibit a single current pulse that quickly follows the zero crossing preceding the positive half-cycle of the driving voltage. Similar behavior is not observed during the negative half-cycle of the voltage waveform, a result attributed to the asymmetric arrangement of the power electrodes of figure 1b. The positive slope of the voltage-current (V-I) characteristics of figure 2b indicates a modest electrical conductivity of the microplasmas, and reflects the operation of the array discharges in the abnormal glow mode. Measurements of the power dissipated by the array find that over 700 mW is consumed by the 16 channels for an RMS current of 0.32 mA. These values contrast with the considerably larger currents drawn by a single jet with a cross-sectional area comparable to the composite area encompassed by the array, suggesting an effective conversion of input electrical power into plasma production and sustenance. Furthermore, this behavior confirms an expected electrical coupling between the plasmas in an array through the capacitive electrode structure of figure 3a and 3b. The microplasma jet arrays of figures 1 and 2 are robust and stable, and measurements of several parameters show them to produce low temperature, non-equilibrium plasmas. Throughout more than one hour of continuous operation, for example, the electrical characteristics of the array are reproducible, and the temperature of the plasma plume near its contact point with the bacterial lawn was found to remain at room temperature (data not shown). Considered together with the power dissipation of the arrays (figure 3c) and the jet emission spectra in the visible and ultraviolet, these results confirm that microplasmas generated in the

array of figure 1 are non-equilibrium and nonthermal. As a result, the effects of the plasma jet array on the downstream bacterial lawn can also be expected to be nonthermal.

Figure 4 is a series of optical micrographs representative of the GFP fluorescence images recorded when L_{cp} (microplasma jet pitch along the horizontal coordinate) = 1 mm. The sample surface area viewed in panels (a) – (d), 880 ×760 μm^2, is larger than that occupied by four microplasma jets and the outlines of the jet positions in figure 4b -4d are indicated by the dashed white circles. Fig. 3a is a fluorescence image of the control (gas flow on but plasmas extinguished) *E. coli* lawn, and panels (b)-(d) illustrate the effect of exposing the *E. coli* lawn to the microplasma array for 1, 2, and 3s, respectively. The darker regions in these images are those in which the *E. coli* bacteria have been deactivated. After 1s of treatment (figure 4b), the deactivated region is approximately the same in area as the jet cross-sections themselves. When the treatment (exposure) time is increased to 2s, however, the deactivated region expands considerably beyond the jet cross-section, giving rise to areas of cell destruction lying along lines connecting the jet axes. Raising the exposure time still further to 3s results in the deactivation region increasing to ~9 times the cross-sectional area of any single jet. If jet-jet interactions are negligible, the cell destruction region is not expected to extend more than 40-50% in diameter beyond that of an individual jet. Our experiments, and those of others with a single jet, confirm this conclusion. Another aspect of figure 4 that should be mentioned is the appearance of small, circular areas of cell deactivation (denoted by red circles in figures 4c and 4d) that are surrounded by a region of living *E. coli* cells and separated spatially from any of the

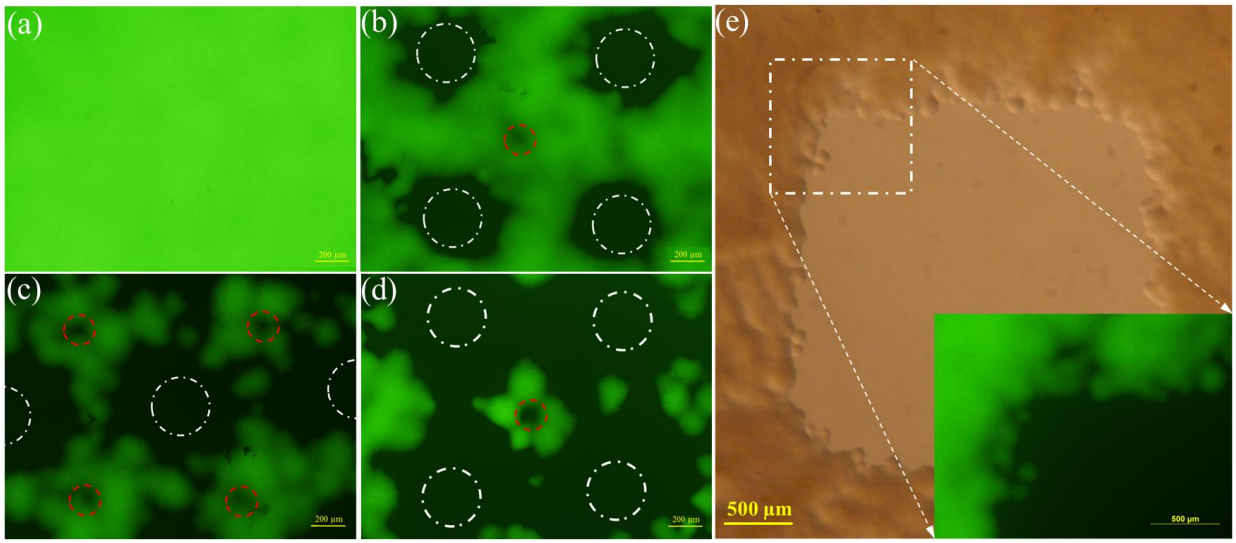

Figure. 4: Optical micrographs of GFP transfected *E. coli* samples before and after exposure to the microplasma jet array; (a) control; (b) exposure of 1s; (c) 2s exposure, and (d) 3s of exposure to the array. In (b)-(d), the locations of the jets within the field of view are indicated by dashed white circles. Panel (e) is an optical microscope image of a GFP-transfected *E. coli* sample after a 5s exposure, confirming bacterial inactivation over the entire portion of the surface defined by the array (the light brown color indicating the area of deactivated E. coli cells and the dark brown the area of the living cells). In recording this image, the surface was *not* illuminated at 483 nm. The inset is a fluorescence image of the upper left-hand corner of a 483 nm-irradiated region of the same sample, demonstrating that the GFP fluorescence images provide an accurate map of the spatial distribution of active *E. coli* cells. For these images, the microchannel pitch along both orthogonal coordinates was set at 1 mm (i.e., $L_{cp} = L_{co} = 1$ mm).

microplasma jets. Lying almost precisely at the geometric center of a group of four jets in figure 4d, for example, this phenomenon is unexpected but reproducible. Because of the centrality (relative to the jet positions) of this circular region of cell deactivation, gas flow effects are presumed to be responsible. Specifically, the fluid dynamics of the flowing He gas in the confined region bordered by four plasma jets gives rise to a quiescent, localized area in which the buildup of long-lived excited species can occur. It is equally possible that heavy particle collisions, such as the conversion of ground state hydroxyl radicals to hydrogen peroxide ($2OH + He \rightarrow H_2O_2 + He$), that are inconsequential within the plasmas themselves, produces several molecules or ionic species that damage the bacterial lawn. Regardless of the relative importance of a simple buildup of long-living species or the secondary production of reactive species physically removed from the microplasma columns, it is clear that the array of multiple microplasma jets facilitates coupling of the reaction chemistry of individual microplasma jets, and that such interactions are likely the cause of chemistry quite different from that occurring within the jets themselves. Similar behavior in a different geometry and over a larger surface area will be discussed later in connection with figure 6.

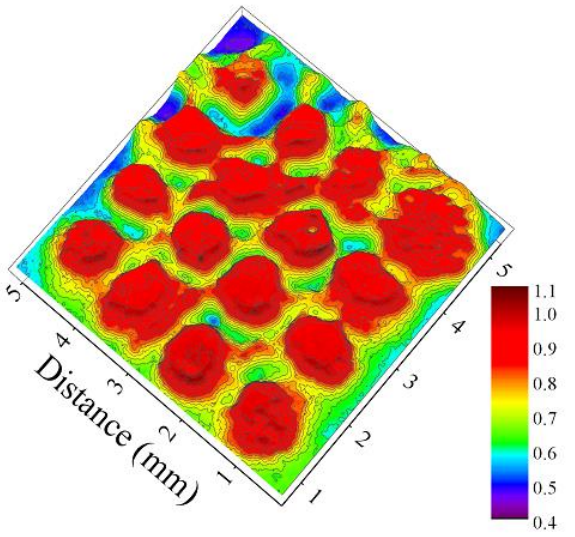

Figure.5 False color image of a lawn of *E. coli* K12 cells that were exposed to the 4 × 4 He microplasma array for 20 s. These *E. coli* cells were not transfected with GFP. The areas shown in red denote the effective deactivation of bacteria and the relative degree of bacterial deactivation is indicated by the color scale at lower right.

In an effort to confirm the reliability of the GFP fluorescence images as an accurate indicator of cell inactivation, images of GFP-transfected cell lawns exposed to blue-green (483 nm) radiation have been compared to those of identical samples for which the transfected bacteria were not photoexcited. One such comparison is presented in part (e) of figure 4. Both of these images were recorded after 5s of exposure of the *E. coli* lawn to the 4 × 4 microplasma array, and microscopic examination shows the entire treatment field to be free of active cells. The larger image of figure 3e is an optical micrograph of the sample in the absence of visible illumination, while the inset shows only a portion of the fluorescence generated when the sample is irradiated at 483 nm. As indicated by the white square in the figure, only the upper left-hand corner of the microplasma treated area of figure 3e is given by the inset but this suffices to demonstrate that the two spatial maps are virtually identical. As noted earlier, experiments similar to those of figure 3 were conducted with normal (non-transfected) *E. coli* K12 cells because of the relative frailty of the GFP-transfected bacteria. Exposed samples were imaged over an area of 6 × 6 mm^2 by conventional light microscopy, and figure 6 is a false color image acquired after an *E. coli* K12 lawn was exposed to the 4 × 4 array for 20s. Despite the increased resistance of the non-transfected cells to the plasma array, the area of cell inactivation associated with each jet is as much as a factor of eight larger than the jet cross-sectional area. Furthermore, evidence in figure 4 of jet-jet interactions in the cell inactivation process is clear.

All of the data presented thus far pertain to arrays for which the microplasma jet pitch along both the horizontal and vertical coordinates was set to 1 mm. If, however, the spacing between the jets is increased within either the rows or columns of the array, spatial modulation of the microplasma-initiated chemistry is observed readily. As an example, figure 6 is a false color image similar to figure 4, and representative of those observed when the center-to-center spacing of the rows is set to 2 mm. This particular spatial map was recorded after 20 s of exposure of the *E. coli* substrate to the array, and the positions of the 16 jets in the array are marked with the dashed white circles. The deactivation of *E. coli* cells over large swaths of substrate area that are well-removed from the nearest row of jets is now quite vivid (as indicated by the red regions of the image). Before discussing these results in more detail, it should be noted that increasing the plasma treatment time to 30s results in the complete deactivation of all bacteria on the agar plate. The small, essentially circular, areas of cell deactivation (discussed earlier with regard to figure 4) are also apparent in the image of figure 6 but the secondary areas of cell destruction (between rows of microplasma jets) are of much greater extent and interest. It must be noted that the deactivation of cells in figure 6 is not continuous along the rows of plasma jets, and yet continuous areas of inactivated cells lying *between* the rows of jets are observed. This phenomenon appears to have not been reported previously but confirms the existence of significant coupling of the reaction chemistry between the individual jets. It is also of interest to note that, between numerous pairs of adjacent jets along at least three of the rows in figure 5, there are areas in which the deactivation is ineffective. In contrast, along the columns (vertical direction), the jet-to-jet distance is twice that for the rows and yet the deactivated areas between rows are larger in extent, and greater in degree (i.e., of darker color), than that within the rows. In comparison with figure 4, therefore, the data of figure 6 offer further support to the proposed influence of secondary reactions in regions physically removed from the jets. We suggest that these results are critical to the future of microplasma jet arrays and their application to plasma processing of substantial surface areas (> a few cm^2).

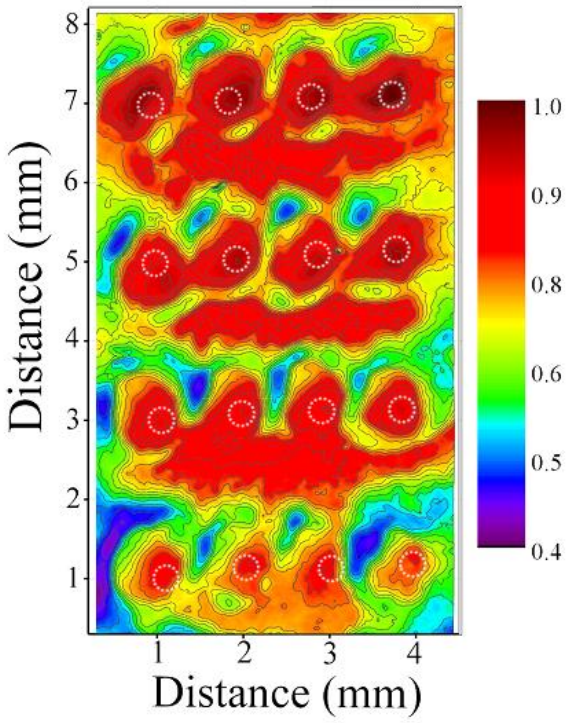

Figure 6 False color image similar to that of Fig. 4 but for a 4 × 4 array in which L_{cp} (horizontal pitch) has been increased to 2 mm. The positions of the 16 jets are indicated by dashed circles.

B. Photon Synergies

A primary focus of the work being conducted at the University of Illinois (UIUC) under this NSF/DOE program is the investigation, under carefully-controlled conditions, of the

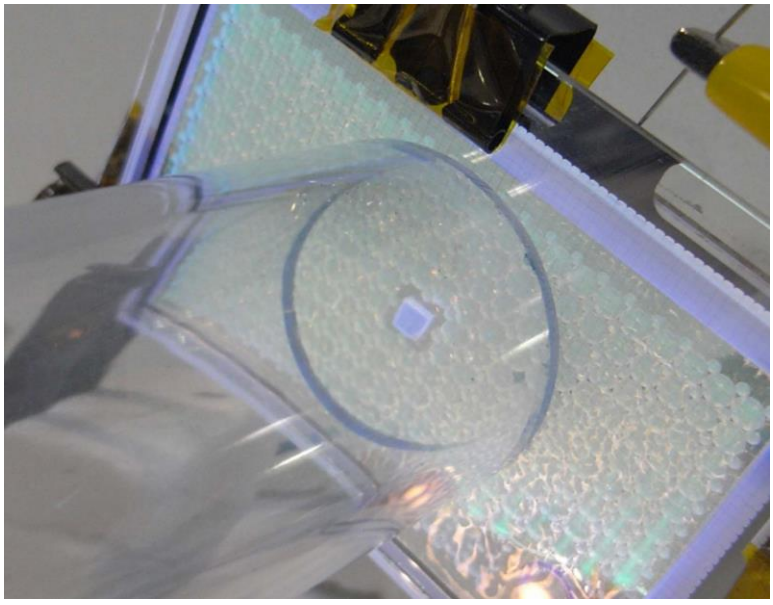

Fig. 7 A Photograph of a VUV transmission test in an ultraviolet-compatible cell designed with a microcavity array operated in Xe. The array of microcavity plasma devices was operated in a Xe/Ne mixture at a pressure of 500 Torr.

synergistic interaction of photons and plasma-produced radicals with a surface. Of particular interest is the use of vacuum ultraviolet (VUV)/UV photons in conjunction with plasma-generated molecular or atomic species, to deactivate bacteria or cells in a spatially-selective manner as described in the last section. A second effort toward that goal is the demonstration, by the research team of University of Illinois and Eden Park Illumination, Inc., of the fabrication of the flat microcavity plasma lamps having an emission wavelength of 172 nm (VUV) which is equivalent to a photon energy of 7.2 eV. We have performed a number of experiments to investigate the dissociation efficiency of those lamps for pathogens and various organic and biomedical substances. Figure 7 is a photograph of the operation of a microcavity array which is connected to the newly-designed, VUV-compatible liquid reaction cell. The microplasma devices are being operated in 500 Torr of a Xe/Ne gas mixture. Fig. 8 shows photographs of the results of experiments for the treatment of a biomedical (hemoglobin) solution by VUV emission produced by microplasma UV lamp. Irradiated over the area of only 1 cm^2, UV emission of ~10 mW/cm^2 was exposed to the solution of hemoglobin (in the concentration of 8 g/liter). Experiments showed that not only decolorization of the solution, but also the complete remediation of the solution was observed less than 1 hour of treatment time. It is also evidenced

Figure 8. Photographs of hemoglobin solution in the concentration of 8 g/l treated for one hour by Vacuum UV (172 nm) emission from microplasma flat lamp. The intensity of UV output was 10 mW/cm^2.

by UV/Vis absorption spectra that samples measured with different treatment time shows significant decrease of hemoglobin absorption peak intensities within 1 hour of irradiation.

III. SUMMARY

The experiments conducted under this NSF/DOE program have demonstrated clearly the benefits of combining efficient sources of UV/VUV radiation with arrays of microcavity plasmas. Arrays of microplasma jets have been shown to deactivate bacteria on a surface quickly, even in regions of the surface on which the jets do not impinge. Secondly, the development of efficient, high power 172 nm lamps has opened the door to a broad range of photochemistries because of the combination of microplasma and VUV sources. We are grateful to the DOE and the NSF for the support of this research!